LED condition monitoring system using U-Net and Luminance Flux Computing Model based on IR thermal images

M. S. KALYANA SUNDARAM[1], J. GNANAVADIVEL[2,*], K. S. KRISHNA VENI[2]
[1]*Department of EEE, AAA College of Engineering and Technology, Tamilnadu, India*
[2]*Department of EEE, Mepco Schenk Engineering College, Tamilnadu, India*

This article introduces an innovative non-invasive method for health status monitoring of industrial LED lighting systems, addressing the need for reliable and efficient maintenance solutions. A combined approach utilizing a U-Net Convolutional Neural Network and a Luminance Flux Computing Model (LFCM) to identify faults in individual LEDs based on computed luminance flux values is proposed. The preprocessing unit designed in this article achieves a Peak Signal-to-Noise Ratio (PSNR) of 40.96 and precise segmentation of LED components using U-Net, achieving an accuracy of 95% and an Intersection over Union (IoU) of 90%. The proposed system effectively estimates the depreciation rate of each LED in a LED panel, providing critical insights into their health and operational efficiency. Performance evaluations reveal the effectiveness of the system and the results are compared with other deep learning techniques such as Fully Convolutional Networks (FCN), Mask R-CNN, SegNet, DeepLabv3+ and PSPNet, highlighting its potential for enhancing the longevity and reliability of industrial LED systems.

(Received October 14, 2024; accepted April 3, 2025)

Keywords: LED health status, Non-invasive method, U-Net, Luminance Flux Computing Model, Thermal imaging, Depreciation rate

1. Introduction

In recent years, Light-Emitting Diode (LED) technology has reached significant growth in demand and applications across multiple industries. From residential and commercial lighting to automotive and signage, LEDs have become ubiquitous due to their energy efficiency, durability and versatility. This widespread adoption underscores the critical role of LEDs in modern industrial settings, where efficient and reliable lighting solutions are essential for productivity, safety and cost-effectiveness. Industries rely on LED panels for plenty of purposes, ranging from general illumination to specialized applications such as display screens, signage and architectural lighting. The advantages offered by LED panels, including flexibility in design, low power consumption and long lifespan, make them an ideal choice for diverse industrial settings. Moreover, the ability to control brightness, colour and intensity adds another dimension of utility, enabling customized lighting solutions tailored to specific requirements. Despite the numerous benefits of LED technology, the reliable operation of LED panels is not immune to challenges. One of the significant challenges faced by industries is the detection of defective LEDs within a panel. Unlike traditional incandescent or fluorescent lights, where a failed bulb is easily noticeable, identifying a malfunctioning LED in a panel poses unique difficulties [1-5]. The inherent nature of LED panels, comprising numerous individual diodes arranged in a grid pattern, complicates the process of pinpointing a defective LED. Moreover, the compact size of LEDs and their integration into complex circuitry make visual inspection alone insufficient for accurate diagnosis [6-8]. Traditional methods for detecting faults in LED lamps often rely on electrical parameter measurements and visual inspections [9]. However, these techniques can be limited in detecting certain types of faults or may not provide comprehensive insights into the performance degradation of the lamps. Existing research highlights the need for more advanced diagnostic techniques that go beyond simple electrical testing and visual observation [10-14]. Time-frequency analysis has been increasingly used in various fields for fault detection and diagnosis due to its ability to capture dynamic changes over time. In the context of LED lamps, analyzing the light output signals using time-frequency methods, such as Variational Mode Decomposition (VMD), can reveal underlying patterns or anomalies that are not visible through traditional methods. Previous studies have shown that time-frequency characteristics can effectively highlight fault signatures and improve diagnostic accuracy. Support Vector Machines (SVM) have been widely employed in fault diagnosis and classification tasks due to their robustness and accuracy. Recent advancements in diagnostic strategies, particularly those combining time-frequency analysis with machine learning techniques, have demonstrated significant improvements in fault detection accuracy [15-18].

But all these methods are invasive, requiring direct access to the LED panel and potentially disrupting ongoing operations [19]. This limitation highlights the need for non-invasive diagnostic techniques capable of accurately identifying LED faults without disrupting normal functioning. Also, identifying defect in a single LED present in the LED panel is tedious.

In response to these challenges, researchers and industry professionals have increasingly turned to infrared (IR) thermal imaging as a promising solution for LED panel fault diagnosis. Thermal imaging is based on the infrared radiation detection to assess temperature variations in objects [20]. Since faulty LEDs often exhibit abnormal heat signatures due to increased resistance or localized overheating, thermal imaging offers a non-destructive and non-contact method for identifying faulty components within an LED panel. Integrating this technology into LED fault detection offers several advantages. Thermal imaging enables rapid and comprehensive inspection of LED panels, allowing operators to identify faulty LEDs with minimal disruption to operations. Also, thermal imaging provides quantitative data on temperature distribution across the panel, facilitating objective analysis and decision-making regarding maintenance or replacement actions. Moreover, thermal imaging offers the capability to detect latent or intermittent faults that may not be apparent through visual inspection or electrical testing alone. By capturing real-time thermal images of LED panels during its operation, thermal imaging systems can identify subtle temperature variations indicative of impending failure or abnormal operation. Additionally, the non-invasive nature of thermal imaging reduces the risk of damage to LED panels during diagnostic procedures, preserving the integrity of the lighting system and minimizing downtime. This aspect is particularly advantageous in critical industrial environments where uninterrupted operation is paramount.

The increasing demand for reliable and efficient lighting solutions in industrial settings underscores the importance of effective LED panel fault diagnosis. While traditional methods face limitations in accurately identifying LED faults, thermal imaging emerges as a promising solution offering non-invasive, real-time and comprehensive fault detection capabilities. By utilizing infrared imaging, industries can improve the reliability, safety and performance of LED lighting systems, leading to increased productivity and cost reductions. While prior studies have explored thermal imaging for LED diagnostics, this research uniquely integrates a U-Net Convolutional Neural Network for precise LED segmentation and a Luminous Flux Computing Model (LFCM) for accurate luminous flux estimation. Unlike traditional fault detection approaches that rely on indirect electrical measurements, this method provides a comprehensive, non-invasive solution capable of real-time fault identification at the individual LED level. Additionally, the proposed preprocessing filter enhances the quality of thermal images by effectively reducing noise while preserving critical details, improving segmentation accuracy. The main highlights of this research includes

- Develop a system capable of accurately detecting faults in individual LEDs within a panel.
- Develop an effective preprocessing filter that excels in preprocessing LED thermal images by effectively reducing noise while preserving important features.
- Implement a U-Net Convolutional Neural Network to provide precise segmentation of thermal images, crucial for isolating and analyzing individual LED components.
- Design a Luminance Flux Computing Model (LFCM) that accurately determines the luminance flux values of individual LEDs within a panel, which are critical for assessing LED performance and health.
- To estimate the depreciation rate of each LED in a LED panel.

2. Proposed system

LEDs consume much less energy than traditional incandescent or fluorescent bulbs. They convert a greater portion of electrical energy into light rather than heat. LED lights are relatively low-maintenance compared to traditional lighting options. The industrial LED lighting systems may be affected due to driver failure, poor heat management and incompatible dimmer. LEDs can experience degradation in brightness and colour over their lifespan. However, addressing the issues proactively can ensure continued performance and longevity. This article is introducing a thermal image based non-invasive technique for finding the luminance flux and depreciation rate of the industrial LED lighting systems. The schematic representation of the proposed system is illustrated in Fig. 1.

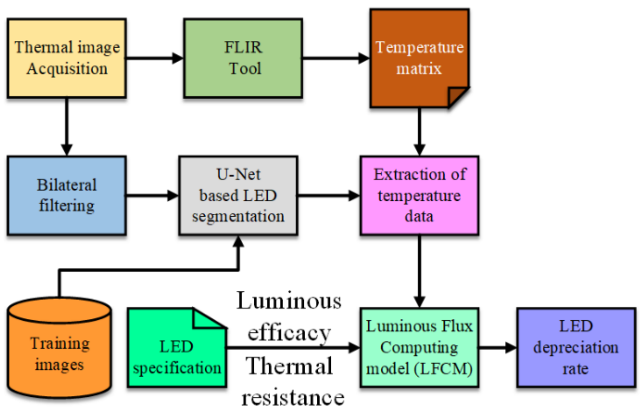

Fig. 1. Schematic representation of the proposed system (colour online)

A. Acquisition of thermal images

The thermal imaging camera detects infrared radiation emitted by LED and converts it into a thermal image, which visually represents the temperature distribution. The thermal image is essentially a matrix where each pixel represents a temperature value corresponding to that particular point. To extract these temperature values, the image is analysed using the FLIR tool software. This software interprets the infrared data and produces a temperature matrix, which quantifies the temperature at each pixel location. The matrix provides a comprehensive view of the temperature distribution across the entire field of view.

B. Preprocessing techniques

Thermal images have less resolution and also, the texture and edge information will not clearly be obtained in a raw thermal image. Certainly, preprocessing techniques are necessary to extract useful information from the image. The primary goal of these techniques is to improve contrast, minimize noise and preserve edge details. The various preprocessing techniques available are given below:

(i) Gaussian filter

The Gaussian filter operates by applying a Gaussian function based convolution kernel. This kernel assigns higher weights to central pixels while gradually decreasing the influence of surrounding pixels, resulting in smooth image filtering. The gaussian function is defined as.

$$G(x,y) = \frac{1}{2\pi\sigma^2} e^{\frac{-x^2+y^2}{2\sigma^2}} \tag{1}$$

where (x,y) are the coordinates of the pixel. σ is the standard deviation, controlling the extent of smoothing. The gaussian filter generates a kernel based on σ. The size of the kernel is typically odd to maintain a center pixel.

(ii) Median Filter

Median filtering is an effective technique for noise reduction in images while preserving edges. Unlike low-pass FIR filters, it maintains edge sharpness, making it particularly useful in image processing for removing 'salt-and-pepper' noise. This method replaces each pixel value with the median of its neighboring pixels, ensuring efficient noise suppression without distorting important details.

(iii) Bilateral filtering

Bilateral filtering is a powerful technique used for image smoothing while preserving edges. It combines domain and range filtering to achieve this effect, making it particularly useful in various applications like image denoising and smoothing. Bilateral filtering operates through a two-step process:

(a) Spatial Component: This is a Gaussian function that considers the distance between pixels in the spatial domain. Pixels closer to the center pixel contribute more to the average.

(b) Range Component: This considers the intensity differences between the center pixel and neighboring pixels, using another Gaussian function. Pixels with similar intensity to the center pixel contribute more significantly.

Mathematically, the output pixel value I'(x) is computed as:

$$\mathrm{I}'(\mathrm{x}) = \frac{1}{\mathrm{W(x)}} \sum_{\mathrm{y}\epsilon\Omega} \mathrm{I(y)}.\, \mathrm{G}_{\sigma_\mathrm{d}}(\|\mathrm{x}-\mathrm{y}\|).\, \mathrm{G}_{\sigma_\mathrm{r}}(-\mathrm{I(y)}) \tag{2}$$

where, W(x) is the normalization factor.

$\mathrm{G}_{\sigma_\mathrm{d}}$ - spatial Gaussian kernel

$\mathrm{G}_{\sigma_\mathrm{r}}$ - the range Gaussian kernel

Ω - is the neighborhood of the pixel x

As the range parameter σ_r increases, the bilateral filter begins to approximate Gaussian convolution due to the broadening and flattening of the range Gaussian, leading to a nearly uniform effect across intensity levels. Meanwhile, increasing the spatial parameter σ_d leads to the smoothing of larger features.

(iv) Non – local diffusion filter

Non-local diffusion filtering reduces noise by averaging pixel values based on their similarity over large regions of the image rather than just local neighborhoods. This allows for effective smoothing while retaining significant details. The output pixel value I'(x) is computed as

$$\mathrm{I}'(\mathrm{x}) = \sum_{\mathrm{y}\epsilon\Omega} \omega(\mathrm{x},\mathrm{y}).\, \mathrm{I(y)} \tag{3}$$

where ω(x,y)is the weight based on similarity. I(y)is the intensity of the neighboring pixel y and Ω represents a search area across the entire image.

C. LED segmentation technique

In this article, the U-Net Conventional Neural network is used to segment LED thermal images. The U-Net architecture is commonly used for the biomedical image segmentation [19] and recently showed better results for the thermal image segmentation [21]. The U-Net architecture consists of two distinct paths such as contracting path and an expanding path. The contracting path, also known as the encoder, consists of layers that extract contextual information while progressively reducing the spatial resolution of the input. Conversely, the expanding path, or decoder, reconstructs the original spatial resolution by decoding the compressed data and incorporating skip connections from the encoder. Through convolutional operations, the contracting path identifies crucial features within the thermal image, reducing spatial dimensions while increasing feature depth to capture more abstract representations. Meanwhile, the expanding path focuses on reconstructing the image by upsampling feature maps and applying convolutional operations. The skip connections between the two paths help preserve spatial details that might otherwise be lost, ensuring precise feature localization during segmentation.

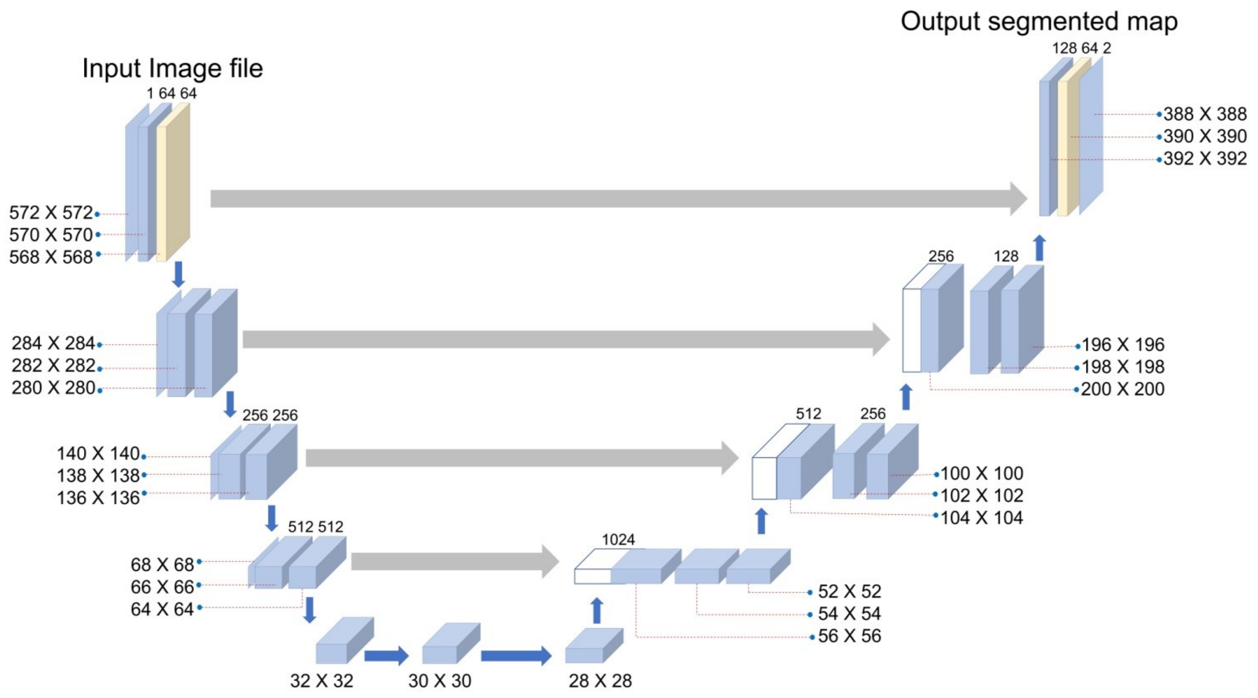

Fig. 2. U-Net architecture for LED segmentation (colour online)

Fig. 2 illustrates the process of segmenting the LED region using U-Net architecture in this work. The grayscale image of size 572×572×1 is given as the input for this network and the final binary segmented output image is extracted with the size of 388×388×2. During encoding, the input image undergoes progressive dimensional reduction, increasing the number of feature channels. This enables the network to extract high-level patterns as it moves deeper. At the bottleneck stage, the feature map is transformed into a 30×30×1024 representation. The decoder then reconstructs the original image size by applying up-sampling layers that restore spatial resolution while reducing the number of channels. Skip connections from the encoder further refine feature localization, ensuring precise segmentation. The final output is a binary segmentation map, where each pixel is classified as either foreground or background.

D. Luminance Flux Computing Model

Luminous flux measures the total amount of visible light emitted by a source in all directions. It quantifies the overall light output without considering the direction or concentration of the light (Lumens - lm) and it is used to describe the total light output of a bulb, LED or other light sources, making it useful in evaluating the efficiency of lighting products. Calculating luminous flux from a thermal image is a complex task because thermal images measure infrared radiation (heat) rather than visible light. However, under certain conditions, it may be possible to estimate luminous flux indirectly, where the heat and light output are related. The novelty in this proposed work is measuring the luminance flux of the LED lights. Meanwhile the traditional methods follow luminance flux measurement with the help of Luminance meter and meanwhile the Luminance will give cumulative luminance flux of the entire LED panel not for the individual LED. The algorithm for the Luminance Flux Computing Model (LFCM) is given below and its individual steps are elaborated in this section.

Step 1: Extraction of Temperature Data:

Convert the thermal image into a temperature matrix T(x,y) where each pixel corresponds to the temperature at that point on the LED array. The LED regions are segmented with the help of U-Net architecture in the previous step. Hence the temperature data are extracted only for the segmented LED region.

Step 2: Calculate Average Temperature

The average operating temperature T_{avg} is computed from the LED temperature matrix

$$T_{avg} = \frac{1}{N}\sum_{x,y} T(x,y) \tag{4}$$

where N is the number of pixels in the LED region and (x,y) represents the pixel coordinates.

Step 3: Estimate Power Dissipated as Heat

The heat power is estimated with the help of the equation given below. Where the thermal resistance R_{th} of the LEDs are available in the LED datasheet. The light power is calculated by subtracting the heat power from the electrical power such as P_{input}.

$$P_{heat} = \frac{T_{avg} - T_{ambient}}{R_{th}} \tag{5}$$

$$P_{Light} = P_{input} - P_{heat} \tag{6}$$

Step 4: Adjust Luminous Efficacy

Luminous efficacy is a temperature dependent parameter and it is provided by the manufacturer. Luminous efficacy quantifies the efficiency of a light source in converting electrical power into visible light. In LED lighting, this efficacy is regulated using a temperature correction factor to account for variations in operating temperature, ensuring optimal performance and efficiency.

$$\eta(T_{LED}) = \eta_{ref} \times TCF \tag{7}$$

$$TCF = 1.0 + \left(\frac{-1}{\eta_{ref}}\right) \times (T_{LED} - T_{ref}) \tag{8}$$

where η_{ref} is the luminous efficacy at the reference temperature and TCF is temperature correction factor.

Step 5: Calculate Luminous Flux

Luminous flux ($\emptyset_v$) can be calculated with the help of following equation where the proposed work is calculating the luminous flux of individual LED segment.

$$\Phi_v = P_{Light} \times \eta(T_{LED}) \tag{9}$$

Step 6: Calculate Depreciation rate

The Depreciation Rate of an LED refers to the reduction in its luminous flux over time. It is often expressed as a percentage and represents how much the LED's light output has decreased compared to its initial value (or expected value).

$$\text{Depreciation rate} = \left(1 - \frac{\text{Calculated Luminous Flux}}{\text{Expected Luminous Flux}}\right) \tag{10}$$

The pseudo code for LFCM is given below,

```
function LFCM (thermal_image, led_specs, power_input, ambint_temp)
returns Luminous_Flux
 # Step 1: Pre-process the thermal image
temperature_matrix⟵thermal_image
# Export using Flir_Tool
led_region = Unet_segmentation(thermal_image)
Temp_over_led_region⟵temperature_matrix∩led_region
# Step 2: Calculate average temperature
T_avg = mean(Temp_over_led_region)
# Step 3: Estimate power dissipated as heat
R_th = led_specs.thermal_resistance
P_heat = (T_avg - ambient_temp) / R_th
P_light = power_input - P_heat
# Step 4: Adjust luminous efficacy based on temperature
eta_ref = led_specs.luminous_efficacy_ref
[pixel_temperature,index]= Temp_over_led_region(:)
functiontemp_correction_function
(ambient_temp, pixel_temperature, eta_ref)
returnstemp_correction_factor
temp_correction_factor=1+(-1/eta_ref)*
(pixel_temperature − ambient_temp)
eta = eta_ref * temp_correction_factor
# Step 5: Calculate luminous flux
Luminous_Flux = P_light * eta
 # Step 6: Calculate Depreciation rate
```

$$\text{Depreciation rate (\%)} = \left(1 - \frac{\text{Calculated Luminous Flux}}{\text{Expected Luminous Flux}}\right) \times 100\ \%$$

3. Results and discussion

The experimental setup for capturing thermal images of LED panel is shown in Fig. 3. The specification of the LED panel is tabulated in Table 1. Also, the thermal images of LED panel array are placed in a closed chamber setup and for various operating voltages such as 25%, 50%, 75% and 100% of rated voltage.

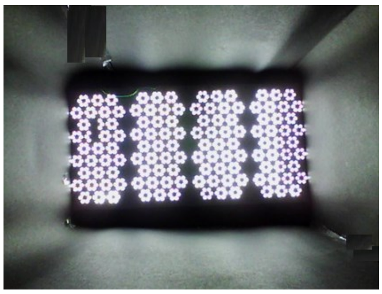

Fig. 3. LED panel in closed chamber setup

The dataset used in this work consists of 3426 thermal images captured from LED panels operating under diverse conditions, including variations in power levels, ambient temperatures, various operating hours (namely 1 hour, 6 hours, 12 hours, 24 hours) and LED aging stages to ensure robustness and generalizability. To evaluate the model's performance across different LED systems, the proposed U-Net segmentation and Luminance Flux Computing

Model (LFCM) were tested on both newly manufactured and aged LED panels. The thermal images are captured using flir thermal C3 Uncooled Microbolometer 640 × 480 pixel with fixed focus camera having spectral range of 7.5 - 14.0 µm and operating temperature of 0 ˚C-150 ˚C. In the closed chamber setup, the LED panel is fully covered with the black body setup and the images are captured with the help of the thermal camera and the captured thermal image is showcased in Fig. 4. The captured thermal images are having poor intensity profile, in order to improve its contrast and to enhance edge information, the preprocessing techniques are implemented in this proposed system. The preprocessing is done with the help of four different methods such as gaussian filter, median filter image, bilateral filter and non-local diffusion filter. Fig. 5 showcases the results obtained from the various preprocessing techniques.

Table 1. Specifications of the LED panel

S. No	Specifications	Ratings
1	Rated voltage	45 V
2	Rated current	650 mA
3	Rated power	30 W
4	Luminous Efficacy	178 lm/W
5	Luminous flux	5345 Lumen
6	Thermal resistance	0.7 ˚C /W
7	Peak Temperature	50 ˚C
8	Number of LEDs	186

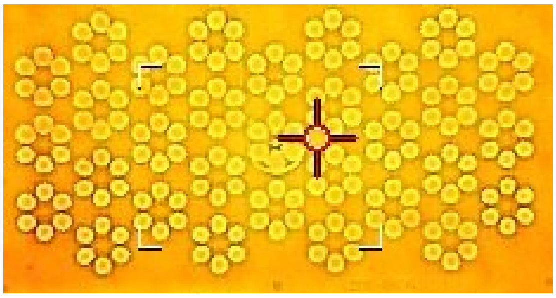

Fig. 4. Captured LED thermal image (colour online)

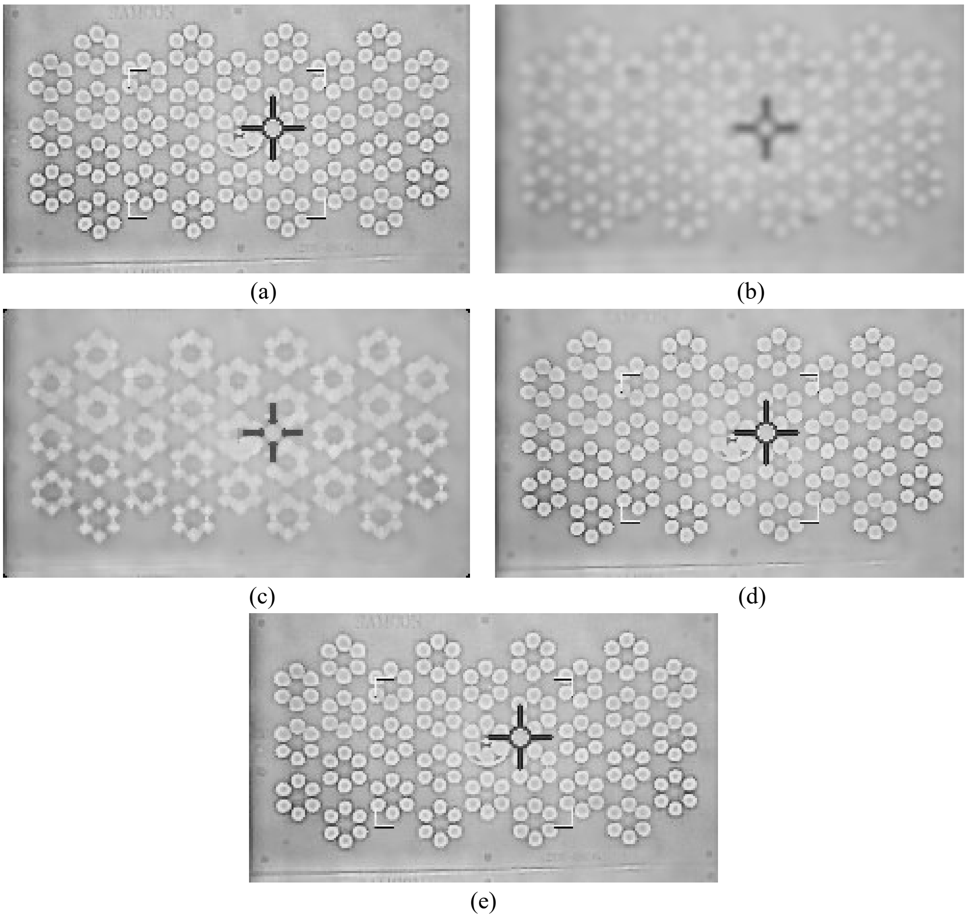

Fig. 5. Preprocessing of thermal images (a) Original thermal image (b) Gaussian filtered image (c) Median filtered image (d) Bilateral filtered image (e) Non-local diffusion filtered image

The performance of different preprocessing techniques is tabulated in Table 2. By evaluating the performance of different pre-processing techniques for LED thermal images, several metrics are used to evaluate their effectiveness. The techniques compared include the bilateral filter, non-local diffusion filter, median filter and Gaussian filter. The bilateral filter emerged as the superior method overall. It achieves the highest Signal-to-Noise Ratio (SNR) and Peak Signal-to-Noise Ratio (PSNR), which indicates excellent noise reduction while preserving image quality. Its Structural Similarity Index (SSIM) is perfect at 1.00, reflecting its capability to maintain the structural integrity of the images. Additionally, the bilateral filter scores highest in Feature Similarity Index (FSIM), underscoring its effectiveness in preserving detailed features. The low Mean Squared Error (MSE), Root Mean Squared Error (RMSE) and Mean Absolute Error (MAE) further validate its strong performance. The non-local diffusion filter also performed well, particularly excelling in PSNR and Edge Preservation Index (EPI). It provides strong noise reduction and edge preservation capabilities, with very low MSE and MAE values. However, FSIM is slightly lower than that of the bilateral filter, indicating marginally less effectiveness in preserving image details. Whereas, the median filter shows less favorable results. It has lower values in SNR, PSNR and SSIM compared to the bilateral and non-local diffusion filters, suggesting that it is less effective at reducing noise and preserving image quality. Its higher MSE, RMSE and MAE values further illustrate its limitations in preprocessing LED thermal images.

Table 2. Performance comparison of various preprocessing techniques

Methods	SNR	MSE	RMSE	PSNR	SSIM	MAE	EPI	VIF	UIQI	FSIM
Gaussian	-3.75	49.40	24.05	31.19	0.53	0.00	0.28	0.37	1.00	0.30
Median	-3.98	36.77	24.70	32.48	0.59	0.16	0.32	0.38	1.00	0.49
Bilateral	13.25	5.24	3.38	40.94	1.00	-0.02	0.93	0.59	1.00	1.19
Non- local	11.21	2.76	4.29	43.73	0.99	0.00	0.89	0.63	1.00	1.04

The gaussian filter performed the least effectively across nearly all metrics. It recorded the highest MSE and RMSE, indicating poor noise reduction and image preservation. The lower SNR and PSNR values highlight its limitations in maintaining image quality compared to other filters. Overall, the bilateral and non-local diffusion filters are the most effective for preprocessing LED thermal images, with the bilateral filter being the preferred choice due to its superior performance across all key metrics. The preprocessed image is converted into gray scale image and it is given as an input for the U-Net architecture. The size of training, validation and testing matrix, is a split of total 3426 images and are taken in the order 70:15:15 during training, validation and testing phase respectively. Fig. 6 shows the segmentation result obtained from the U-Net architecture. The result is in the form of binary where the white pixels represent the LED region and black pixels represent the non-LED region.

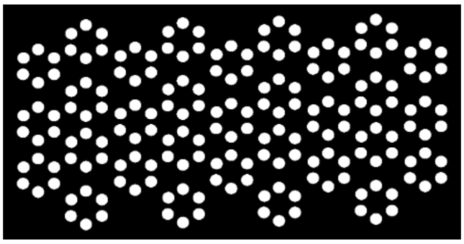

Fig. 6. U-Net Segmented LED image

Table 3. Performance comparison of various segmentation techniques

Method	Accuracy (%)	IoU (%)	Dice Coefficient	Processing Time (ms)	Parameter
U-Net	**95**	**90**	**0.88**	**120**	**31.03M**
FCN	92	85	0.81	150	134.7M
Mask R-CNN	94	89	0.85	200	44.7M
SegNet	90	80	0.78	130	29.5M
DeepLab v3+	93	87	0.83	110	40M
PSPNet	92	86	0.82	170	50M

Accuracy measures the percentage of correctly predicted pixels in the image. From the Table 3 it is evident that the U-Net delivers the highest accuracy at 95%, making it more efficient than other segmentation techniques. Further analysis of fault detection accuracy showed 96% precision for early-stage degradation, 94% for partial malfunctions and 91% for full LED failures. These results confirm the system's reliability in real-world scenarios and its ability to generalize across various LED fault conditions. The dice coefficient metric is used for evaluating the segmentation performance and it measures the similarity between predicted and actual regions. U-Net has the highest dice coefficient of 0.88, indicating highly accurate segmentation predictions. IoU measures the overlap between the predicted and ground truth segmentation and higher IoU reflects better segmentation. U-Net achieves the best IoU at 90%, indicating a high overlap between predicted and actual regions. Processing time is very important parameter for real-time applications. DeepLabv3+ offers the fastest processing time at 110 ms, making it the most efficient in terms of speed. U-Net follows closely at 120 ms, also offering fast processing. The number of parameters is an indicator of the model's complexity and potential resource usage. FCN has the highest number of parameters at 134.7M, making it a very resource-intensive model. U-Net and SegNet are the most efficient in terms of parameter count, with 31.03M and 29.5M parameters, respectively. The proposed U-Net segmentation stands out as the top performer with the best accuracy, IoU and Dice coefficient, while maintaining a reasonable processing time and parameter count. The temperature values of each LED pixel value are extracted from the temperature matrix computed by the FLIR software. The extracted temperature is given as the input for the LFCM and the parameters calculated in the LFCM is shown in Table 4. To showcase the test results, the luminous flux values and depreciation rate of 10 LEDs in a panel is shown in Table 5.

Table 4. Computed thermal parameters using LFCM

Parameters	Values
Average temperature	38.28℃
Electrical Power (P_{in})	30W
Heat Power (P_{heat})	18.97W
Light Power (P_{light})	11.02W
Luminous Efficacy (η_{ref})	173 Lm/W

Table 5. Sample computed Luminous flux (Lumen) values of individual LEDs

LED index	Luminous Flux in Lumen	Depreciation Rate (%)
1	12.72709	55.71123
2	10.37252	63.90483
3	27.72575	3.517623
4	10.84966	62.24446
5	11.46164	60.11484
6	10.06135	64.98769
7	26.43956	7.993423
8	8.92037	68.95816
9	27.17601	5.430667
10	9.760544	66.03445

The proposed system is capable of computing the depreciation rate of each LEDs present in the panel based on the current luminous flux of the LED segments as shown in Fig. 7. Since operating voltage is considered during the luminous calculation, the computed depreciation rates are accurate. Higher the depreciation rate, the condition of LED is bad and needs consideration. Lower the value indicates the better performance of LED. In Fig. 7(a), the green colour circle represents LED operating under normal operating conditions with minimum depreciation rate. Whereas in the Fig. 7(b), red colour circles represents the deprecated LED, it shows the reduced luminous value. Fig. 7(c) shows some LEDs are faulty and it is denoted by gray colour, which means no light output from the corresponding LEDs. The proposed LFCM algorithm is validated on different aged single LEDs and the actual luminous flux of the test LED is measured with the help of lux meter and the LFCM. For this validation, different aged single LEDs i.e., 60 days (1,440 operating hours), 120 days (2,880 operating hours) and 300 days (4,320 operating hours) are tested. Table 6 represents the luminous flux values calculated with the help of LFCM and conventional method using lux meter. The comparison of the results reveals that the LFCM algorithm performs remarkably well, with minimal deviation from the lux meter measurements. The Mean Squared Error (MSE) between the two methods is as low as 0.1 which demonstrates that the LFCM algorithm is nearly identical to the conventional method in calculating luminous flux.

Table 6. Performance evaluation of LFCM

Age of the LED	Index of the LED	Luminous Flux (LFCM Algorithm)	Luminous Flux (Lux Meter)	Error (Flux Difference)
60 days	LED1	95.4 lm	96.0 lm	0.6 lm
	LED2	94.2 lm	94.5 lm	0.3 lm
	LED3	96.8 lm	97.0 lm	0.2 lm
120 days	LED1	92.5 lm	92.1 lm	0.4lm
	LED2	91.9 lm	91.8 lm	0.1 lm
	LED3	93.5 lm	93.9 lm	0.4 lm
180 days	LED1	89.5 lm	89.7 lm	0.2 lm
	LED2	89.0 lm	88.5 lm	0.5 lm
	LED3	90.9 lm	90.8 lm	0.1 lm

The performance of the proposed system is evaluated by comparing with other methods addressed in the literature and it is tabulated in Table 7. The proposed method utilizes a U-Net and Luminance Flux Computing Model, which allows for non-invasive analysis and the ability to assess the luminous output of individual LEDs. Unlike the other methods, which are primarily invasive and focus on online or offline diagnosis, this approach supports both online and offline assessments, enhancing its versatility. Additionally, it uniquely computes the depreciation rate, providing valuable insights into the lifespan and performance of the LEDs, which is not addressed by the other methods.

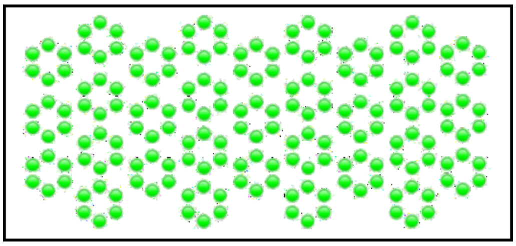

(a)

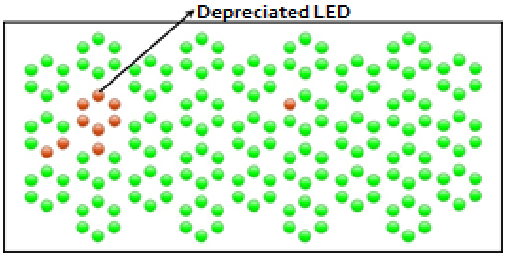

(b)

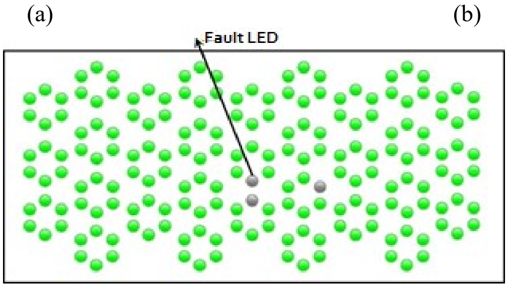

(c)

Fig. 7. Health status of LED (a) Normal condition (b) Panels with depreciating LEDs (c) Panel with faulty LED (colour online)

Table 7. Performance comparison of proposed system with other methodologies available in the literature

Parameters	**Proposed Method**	**[11]**	**[12]**	**[13]**
Method used	U-Net, LFCM	SVM	Life prediction model	PWM control
Computational parameter	IR thermal image	Electrical	Temperature	Electrical
Invasive / Non-Invasive	Non-Invasive	Invasive	Invasive	Invasive
Data fusion	Not required	NA	Required	NA
Online/ Offline	Both	Online	Online	Offline
Capability of computing individual LED luminous	Yes	No	No	No
Depreciation rate calculated	Yes	No	No	No

4. Conclusions

The proposed LED health monitoring system offers a robust and non-invasive solution for monitoring and assessing the health of industrial LED lighting systems. The results indicate that the U-Net model achieved an accuracy of 95% and a Dice coefficient of 0.88, significantly outperforming other segmentation algorithms such as FCN and Mask R-CNN, which achieved accuracies of 92% and 94% respectively. The Luminance Flux Computing Model provides accurate depreciation rate estimations, with observed values indicating that higher depreciation rates correlate with a 30% reduction in luminous output. From an industrial perspective, this work contributes to minimizing downtime and operational costs by facilitating real-time LED health assessments. The non-invasive nature of thermal imaging ensures that LED panels can be monitored without physical intervention, reducing the risk of damage during diagnostics. Furthermore, the ability to estimate individual LED depreciation rates allows industries to plan maintenance schedules more efficiently, extending the overall lifespan of LED systems. Beyond immediate applications, this research lays the foundation for further advancements in LED technology, particularly in the development of intelligent lighting systems equipped with automated fault detection. Future integration with IoT-based monitoring platforms could enable large-scale deployment in smart factories and infrastructure, improving energy efficiency and sustainability.

References

[1] V. Gupta, B. Basak, B. Roy, IEEE Calcutta Conference (CALCON), 462 (2020).

[2] J. Gnanavadivel, N. Senthil Kumar, C. N. Naga Priya, S. T. Jaya Christa, K. S. Krishna Veni, J. Optoelectron. Adv. M. **18**(11-12), 1007 (2016).

[3] J. Gnanavadivel, N. Senthil Kumar, P. Yogalakshmi, J. Optoelectron. Adv. M. **18**(5-6), 459 (2016).

[4] Y. Lin, S. Pan, J. Yu, Y. Hong, F. Wang, J. Tang, S. Chen, Computers in Industry **164**, 104204 (2025).

[5] O. F. Farsakoglu, H. Y. Hasirci, J. Optoelectron. Adv. M. **17**(5-6), 816 (2015).

[6] F. Sun, X. Zhuo, Q. Fang, J. Xie, Optik **193**, 163023 (2019).

[7] S. M. Mizanur Rahman, J. Kim, G. Lerondel, Y. Bouzidi, K. Nomenyo, L. Clerget, Resources, Conservation and Recycling **127**, 256 (2017).

[8] H. Chen, J. J. Lin, IEEE International Conference on Prognostics and Health Management (ICPHM), 231 (2024).

[9] Pawel Zajac, Grzegorz Przybylek, Engineering Failure Analysis **115**, 104693 (2020).

[10] B. Sun, X. Jiang, K. C. Yung, J. Fan, M. Pecht, IEEE Transaction on Power Electronics **32**(8), 6338 (2017).

[11] Sun Bo, Xuejun Fan, Huaiyu Ye, Jiajie Fan, Cheng Qian, Williem van Driel, Guoqi Zhang, Reliab. Eng. Syst. Safe. **163**, 14 (2017).

[12] Alexander Herzog, Simon Benkner, Babak Zandi, Matteo Buffolo, IEEE Access **11**, 19928 (2023).

[13] Bo Sun, Y. Shen, Z. Zhang, C. Guo, C. Cui, Microelectron Reliab. **142**, 114904 (2023).

[14] Chen Gong, H. Xu, J. Liang, Z. Yuan, X. Chen, H. Li, AOPC 2022: Optoelectronics and Nanophotonics, Proc. SPIE **12556** (2023).

[15] Yuhang Shang, Fukang Sun, Qiansheng Fang, Bailing Chen, Jianxia Xie, Heliyon **9**(9), 19737 (2023).

[16] G. Sun, Y. Bai, Z. Zhang Frontiers in Sustainable Energy Policy **3**, 1343339 (2024).

[17] M. C. Moolman, W. D. Koek, H. P. Urbach, Opt. Express **17**, 17457 (2009).

[18] Y. Lee, H. Zhang, J. Rosa, IOP Conference Series: Materials Science and Engineering **490**(4), 042053 (2019).

[19] O. Ronneberger, P. Fischer, T. Brox, Medical Image Computing and Computer-Assisted Intervention, Springer, 234 (2015).

[20] K. S. Krishna Veni, N. Senthil Kumar, J. Gnanavadivel, Electr. Eng. Preprint (2024).

[21] M. Siami, T. Barszcz, R. Zimroz, Scientific Reports **24**(11), 5748 (2024).

*Corresponding author: gvadivel@mepcoeng.ac.in